Contents lists available at: http://qu.edu.iq

Al-Qadisiyah Journal for Engineering Sciences

Journal homepage: https://qjes.qu.edu.iq

Research Paper

Check for updates

Investigation of near field distributions of meander line antenna in human body conditions

Ngu War Hlaing [1], ***Kamilia Kamardin*** [2,3], ***Yoshihide Yamada*** [2], ***and Angela Amphawan*** [1]

[1] *Faculty of Engineering and Technology, Sunway University, Jalan Universiti, Bandar Sunway, 47500 Petaling Jaya, Selangor, Malaysia.*
[2] *Malaysia-Japan International Institute of Technology, Universiti Teknologi Malaysia, Jalan Sultan Yahya Petra, Kampung Datuk Keramat, 54100 Kuala Lumpur, Malaysia.*
[3] *Malaysia Wireless Communication Center, Universiti Teknologi Malaysia, 80990 Johor Bahru, Johor, Malaysia.*

ARTICLE INFO

Article history:
Received 05 April 2025
Received in revised form 14 January 2026
Accepted 7 June 2026

keyword:
Meander line antenna (MLA)
Electric-field pattern
Propagation loss
Electric field deterioration
Healthcare uses

ABSTRACT

Understanding the near-field distribution of antennas has become more significant since it directly effects radiation performance, energy absorption, and safety in current wireless applications, especially when antennas operate close to the human body. This research explores a Meander Line Antenna (MLA)'s electric field patterns within in-body contexts, emphasizing propagation loss, energy conservation, and electric field deterioration in different physiological tissues. This investigation examines the process of signal weakening in embedded antenna use by assessing the variations in electric field strengths among Muscular tissue, skin, and fatty layers at diverse conductivity levels. By utilizing results from FEKO simulations, the research demonstrates the absorption losses associated with the electric field distribution across tissue surfaces. The findings indicate these tissue components exhibiting higher electrical conductance, such as muscle and skin, experience faster degradation when subjected to electric fields compared to fat, which possess lower dielectric constant. These results provide crucial insights into effectively optimizing MLA structure for medical purposes, ensuring reliable wireless signal transfer in physiological environments.

1. Introduction

In recent periods, a notable rise occurs in the surrounding implantable wireless sensors, particularly in their exploration for medical uses. Early detection of illnesses, notably chronic diseases, is among the numerous potential biomedical applications for these technologies [1]. Due to continuous observation of their behavior in routine physiological conditions, patients experience a notable enhancement in their quality of life when they can participate in everyday activities rather than being confined to bed or a wheelchair. Consequently, the ability to monitor patients in their daily routines is the most significant benefit. As a result, conventional clinical monitoring would be substituted with continuous, remote monitoring [2]. This will significantly promote a better lifestyle, increase the accuracy of diagnoses, and reduce health care costs. Figure 1 displays the implantable medical devices' schematic diagram. Understanding energy propagation and signal attenuation requires examining the electric-field patterns of meander line antennas (MLA), considering in-body, essential for biomedical and wireless implantable applications [3]. The efficacy of antenna performance in biological settings has emerged as a vital area of research due to the rising use of implanted and wearable medical devices for live medical status tracking [4]. Nevertheless, the intricate electromagnetic interactions between the antenna and biological tissues lead to challenges such as energy absorption, propagation loss, and field degradation [5]. These concerns impact signal efficacy and overall system reliability [6]. This study looks at how the near-field of MLA implanted in fat, muscle, and skin varies depending on conductivity. The study examines how tissue conductivity influences efficient energy utilization, signal attenuation, and field strength [7]. The study explains how conductivity and permittivity affect signal intensity and propagation characteristics under physiological settings by examining how electric fields deteriorate in various tissue environments. A numerical and simulation-based method is used to determine the near-field pattern at the phantom and antenna interfaces. The propagation loss is measured by the ratio of the surface area covered by the electric field, whereas the absorption loss caused by biological tissues is examined using degradation constants [8]. Furthermore, this thinks about contrast situations with elevated electrical conductivity, which result in prominent electric field weakening, with fat, which has lower conductivity and permittivity [9]. Furthermore, this study compares settings with lower conductivity and permittivity—fat—with those with higher conductivity, such as muscle and skin, which result in greater attenuation of electric fields [10]. The inadequacy of energy conservation models in high-permittivity media, such as human tissue, which leads to significant propagation losses and electric field degradation, is one of the several challenges faced in previous research on implanted antenna systems [11]. For instance, earlier studies sometimes employed simple phantom models that failed to account for the complex dielectric properties of actual tissues, resulting in erroneous performance predictions and exaggerated antenna efficacy. Additionally, several published studies failed to consider the impact of proximal field interaction between the antenna and the tissue, leading to increased absorption losses and less-than-ideal radiation patterns [12]. The development of dependable and efficient WBAN systems was hampered by these limitations. Unlike many prior studies on implantable and wearable antennas that primarily emphasize resonance behavior, impedance matching, or specific absorption rate (SAR), this work focuses on the quantitative characterization of near-field electric-field degradation in biological tissues.

*Corresponding Author.
E-mail address: warhlaingn@sunway.edu.my ; Tel: (+60) 111-205 6376 (Ngu Hlaing)

https://doi.org/10.30772/qjes.2026.165671.1756

Nomenclature

MLA	Meander Line Antenna	X_D	Capacitive reactance (Ω)
E_1	Electric field at antenna–tissue interface ($d\,BV/m$)	N	Number of meander turns
E_2	Electric field at observation point ($d\,BV/m$)	W	Antenna width (mm)
S_A	Surface area of antenna field distribution (mm^2)	H	Phantom height (mm)
S_P	Surface area of phantom field distribution (mm^2)	P_{loss}	Power dissipation density (W/m^3)
L_Z	Absorption loss (dB)	*Greek Symbols*	
b	Electric field degradation constant (Np/m)	σ	Electrical conductivity (S/m)
L	Antenna length (mm)	ε_r	Relative permittivity
D	Phantom diameter (mm)	ε	Absolute permittivity (F/m)
Z_{in}	Input impedance	λ_o	Free-space wavelength (mm)
R_D	Radiation resistance of short dipole (Ω)	λ_g	Wavelength in tissue medium (mm)
R_L	Ohmic resistance of conductor (Ω)	ω	Angular frequency (rad/s)
X_C	Inductive reactance (Ω)	δ	Loss tangent angle

A surface-area–based propagation loss framework (S_A/S_P) is employed to explicitly relate electric-field spreading and attenuation to tissue electromagnetic properties. By analyzing a compact meander line antenna (MLA) operating at 405 MHz within fat, skin, and muscle under identical antenna geometry, excitation, and propagation depth, this study isolates the influence of tissue conductivity and permittivity on near-field degradation. The proposed approach is validated through full-wave FEKO simulations and provides explicit numerical metrics of electric-field loss (dB) and attenuation constants, offering a more quantitative and physically interpretable basis for evaluating implantable antenna performance in wireless body-area network (WBAN) applications.

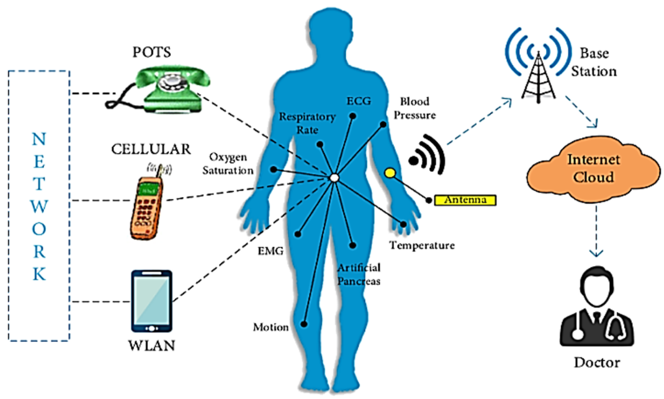

Figure 1. Network of Implantable Medical Devices [13].

2. Design consideration for meander line antenna

The MLA adds resonances that are far lower in magnitude than a standalone antenna element of the same length, extending the spectral span of the conventional folding antenna significantly. In contrast to traditional quarter-wavelength and mid-wavelength dipole antennas, the MLAs' radiation efficiency is significantly lower. The main factors influencing the proportional size decrease of the antenna are the number of meander sections within a single wavelength and the gap between the widths of the rectangular configurations. Figure 2 depicts an equivalent meander line antenna model, Eq. 1.

$$Z_{in} = R_D + R_L + j(X_c - X_D) \tag{1}$$

In this context, X_D denotes the capacitive opposition to current (reactance) of the short dipole antenna, while X_C refers to the inductive reactance introduced by the bent segment (crank). R_D and R_L represent the radiated resistance of the short dipole and the ohmic resistance of the antenna conductor, respectively. The values of X_C and X_D can be neutralized by appropriately choosing the width (W), length (L), and the number of windings (N). Achieving zero net reactance, referred to as the self-resonant state, is crucial for efficient electromagnetic radiation. W changed at fixed L and N until the resonance point was found by moving the 405MHz location to $X = 0.W$ is currently known as the antenna's resonant width. A self-resonant structure curve is obtained by repeating the process for different L and N conditions. As the number of rotations rises, the antenna's size will also grow. In this project, we aim to develop the smallest antenna feasible. For this reason, $N = 6$ is chosen.

3. Simulation model and parameters

The MLA was modeled for implantable uses in the human body. Three parts of the human body—the skin, fat, and muscle were so chosen. The purpose is to examine how well MLA performs at different conductivity and permittivity levels. The simulation model produced with FEKO 7.0, an electromagnetic simulation program, is shown in Fig. 3. In this research, the phantom size is $(80 \times 70 \times 70)\ mm^3$ for fabrication and measurement convenience. Simulation of MLA with different phantom sizes is tested, and the antenna performance shows no significant difference. However, the phantom size should not be smaller than twice the antenna size [14]. To ensure numerical accuracy, the dielectric properties and attenuation behaviour obtained from the FEKO simulations were compared against established biological tissue data reported by Gabriel et al. (1996), [15]. The simulated trends in electric field degradation across fat tissue showed close agreement with published dielectric constants and attenuation characteristics at comparable frequencies, providing confidence in the simulation accuracy. The simulation model's parameter values are compiled in Table 1. For calculating close and far field zones for simulation, this is a suitable size. A $1mm$ air gap is positioned between the antenna and the dielectric material to prevent modeling errors. A computational method, as per the Method of Moments (MoM), will be applied for estimating the electrical characteristics of MLA within the body tissue equivalent material. As mentioned earlier, MoM is a computation that is based on the current flowing through a material or antenna wire that is separated into tiny meshes in the shape of triangles. A mesh convergence assessment was conducted by refining the discretization beyond $\lambda g/150$ for conductors and $\lambda g/20$ for dielectric regions, with no significant variation observed in the near-field electric field magnitude or attenuation trends. Hence, the selected mesh parameters were deemed sufficient for stable and reliable simulations.

4. Power conservation principles and attenuation effects

In the reactive near-field region of an electrically small implantable antenna, electric-field attenuation is governed by two dominant mechanisms: (i) geometric field spreading, which redistributes electromagnetic energy over an increasing effective surface area, and (ii) material absorption, arising from conductive and dielectric losses in biological tissues. Rather than representing far-field path loss, the present analysis models near-field attenuation as a phenomenological superposition of these two effects, consistent with energy conservation principles in lossy media. The energy conservation of the phantom and antenna is investigated. Propagation loss, which is the weakening of signal strength once transmitted across a specific environment and range, is another name for the acquired power at two different locations inside the field generated by electromagnetic sources. Accordingly, the near-field propagation loss between the antenna–tissue interface and a specified observation point within the phantom is expressed as the sum of a geometric spreading term and an absorption-related attenuation term, as given in Eq. 2, [16].

$$Propagation\ loss = E_2 + E_1 = \frac{S_A}{S_P} + L_Z \tag{2}$$

In Eq. 2 the electric-field quantities E_1 and E_2 represent the magnitudes of the electric field at the antenna-tissue interface and at the observation location within the phantom, respectively. All field quantities are expressed in decibel scale (dBV/m), such that subtraction corresponds to a logarithmic field ratio. The term S_A represents a dimensionless surface-area ratio that accounts for geometric redistribution of the near-field energy, while L_Z represents the material absorption loss (dB) accumulated over the propagation depth Z. Although the surface-area ratio originates from linear geometric considerations, its contribution is expressed in logarithmic form using 10 $log_{10}(S_A/S_P)$ to ensure dimensional consistency with the field attenuation expressed in dB.

Table 1. Simulation parameter

Parameter	Value
Simulator	FEKO 7.0 (Method of Moment)
Frequency	405 MHz
Wavelength in free space (λo)	λo =740 mm
Width of the conductor (d)	d = 0.08, 0.1 mm, and 0.5 mm
Number of turns (N)	N = 6
Metallic conductor material	Copper ($\sigma_c = 5.8 \times 10^8\ S/m$)
The dielectric constant of mean fat tissue	Target Value Conductivity of Fat (σ) = 0.193 S/m Permittivity of Fat (ε_r) = 12.21 F/m Wavelength in (λg) = 211.7 mm
The dielectric constant of skin	Target Value Conductivity of skin (σ) = 0.69 S/m Permittivity of skin (ε_r) = 46.7 F/m Wavelength in (λg) = 108.4 mm
The dielectric constant of muscle	Target Value Conductivity of skin (σ) = 0.79 S/m Permittivity of skin (ε_r) = 57 F/m Wavelength in (λg) = 98 mm
Mesh size	$\lambda g/150$ (conductor),$\lambda g/20$ (dielectric)
Substrate (only used in the body)	Teflon Permittivity ε_r = 2.1 Thickness t = 0.25 mm Loss tangent δ = 0.0008

4.1 Calculation of surface area

The cylindrical-shaped embedded antenna SA and the elliptically shaped phantom SP by using Eqs. 3 and 4 are shown below [16].

$$S_A = L(mm) \times W(mm) \tag{3}$$

$$S_P = H(mm) \times D(mm) \times \pi \tag{4}$$

Where H is the height of the cylindrical phantom and D is the diameter of the cylindrical phantom. The ratio of the surface distribution of the electric field is determined in Eqs. 5, Eq. 6, and Eq. 7. Table 2 outlines the results of the electric field propagation.

Table 2. Electric field spatial spread overview.

Parameter	Muscle	Skin	Fat
L (mm)	04.90	05.42	10.60
W(mm)	06.80	07.18	17.70
S_A (mm)	33.32	38.92	187.62
H_P (mm)	70.00	70.00	70.00
D_P (mm)	80.00	80.00	80.00
S_P (mm)	5600 π	5600 π	5600 π
S_P/S_A	505.68	452.03	93.76
10 log (S_P/S_A) dB	27.00	26.60	19.72

$$P_1 = W_1 = E_1 \times H\frac{E_1^2}{Z_o} \tag{5}$$

$$S_A = \frac{E_2^2}{Z_o}S_P = \frac{E_1^2}{Z_o} \tag{6}$$

$$\frac{E_2^2}{E_1^2} = \frac{S_A}{S_P} = -27dB \tag{7}$$

4.2 Electric field degradation in different conductivities

The variations in E-fields in different conductivities are depicted in Figs. 4, 5, and 6, and the simulation results may be used to calculate E-field degradation values. The distribution when conductivity is zero is shown in Figure 4. While the phantom produces 24 $dB\ V/m$, the antenna's highest E-field produces 51 $dB\ V/m$. The LZ value is zero since conductivity is zero [17]. E-field deterioration (E2-E1) is therefore -27 $dB\ V/m$.

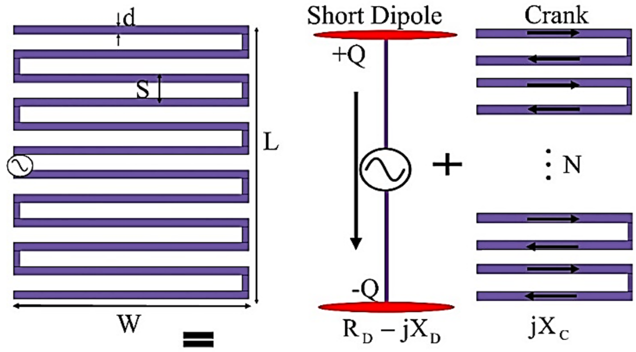

Figure 2. Analytical equivalent current representation of the MLA.

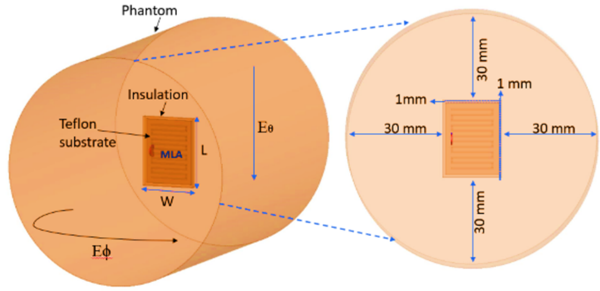

Figure 3. Simulation model of MLA in human body condition.

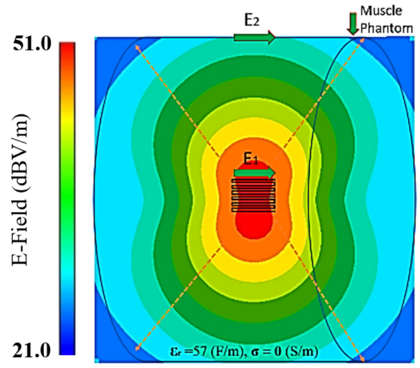

(a) Model with $\varepsilon_r = 57(F/m)$, $\sigma = 0(S/m)$

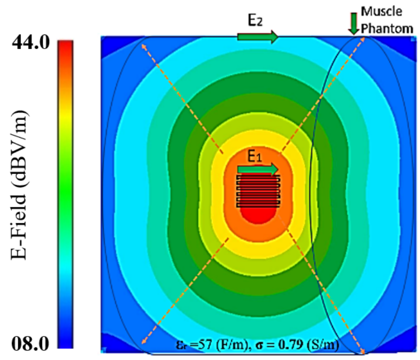

(b) Model with $\varepsilon_r = 57(F/m)$, $\sigma = 0.79(S/m)$

Figure 4. Near field distribution of MLA in muscle.

The highest E-field will be 44 dB V/m for $\sigma = 0.79$ for the antenna, whereas phantom results in 22 $dB\ V/m$ at muscle. E-field deterioration has a value of -32 $dB\ V/m$. Therefore, under muscular circumstances, more conductivity may result in more electric field deterioration. The highest E-field for MLA produces 70 $dB\ V/m$ and phantom produces 42 $dB\ V/m$ for the electric field pattern with zero conductivity depicted in Fig. 5. L_Z value is 0 since the conductivity is zero. E-field deterioration is therefore -28 $dB\ V/m$.

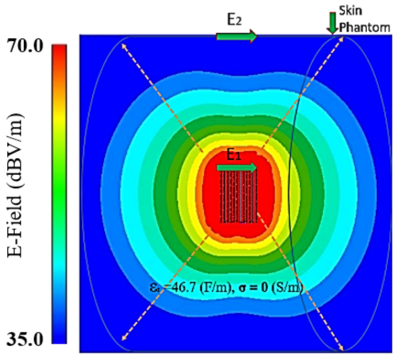

(a) Model with $\varepsilon_r = 46.7(F/m)$, $\sigma = 0(S/m)$

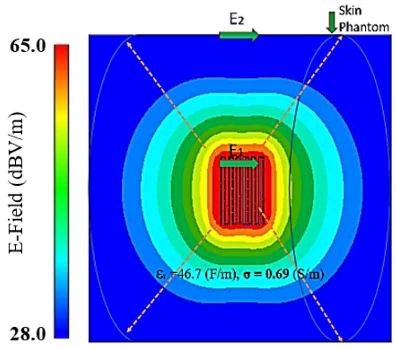

(b) Model with $\varepsilon_r = 46.7(F/m)$, $\sigma = 0.69(S/m)$

Figure 5. Near field distribution of MLA in Muscle.

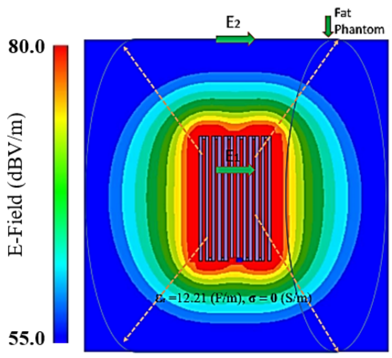

(a) Model with $\varepsilon_r = 12.21(F/m)$, $\sigma = 0(S/m)$

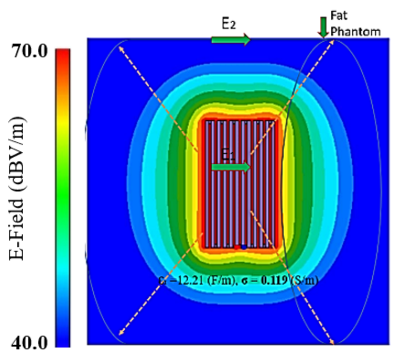

(b) Model with $\varepsilon_r = 12.21(F/m)$, $\sigma = 0.119(S/m)$

Figure 6. Near field distribution of MLA in Muscle.

The strongest electric field is 65 $dB\ V/m$ for σ = 0.69 at the antenna side, whereas the phantom results in 35 dB V/m at the skin. E-field degradation ($E_2 - E_1$) has a value of -30 $dB\ V/m$. Therefore, in skin circumstances, more conductivity may result in more electric field deterioration. The highest E-field at the antenna will produce 80 $dB\ V/m$ for the pattern of electric field in absence of conductivity depicted in Fig. 6, whereas the phantom will produce 60 $dB\ V/m$ at the fat. L_Z value is 0 since the conductivity is zero. E-field deterioration is therefore -20 $dB\ V/m$.

4.3 Absorption loss by human body condition

The maximal E-field will be 70 $dB\ V/m$ for σ = 0.119 for the antenna side, while the phantom produces 46 $dB\ V/m$ for the fat. E-field deterioration ($E_2 - E_1$) has a value of -24 $dB\ V/m$. Therefore, in fat circumstances, more conductivity may result in more electric field deterioration. The attenuation ($S_A/S_P + L_Z$) can be calculated by using the attenuation caused by the human body condition. To evaluate the decline in E-field, the degradation constant B, Eq. 8.

$$B = \frac{\sqrt{2\pi}}{\lambda g}\sqrt{\sqrt{1+\frac{(60\lambda g\sigma)^2}{\varepsilon_r}}-1} \tag{8}$$

At the phantom situated 35 mm from the antenna structure, the electric field degradation can be seen by Eq. 9.

$$L_Z = 10\log(e^{-2bz}) \tag{9}$$

The phantom's electric field deterioration is denoted by L_Z. Table 3 shows the E-field losses measured in structure A's muscle, skin, and fat. When fat has low conductivity and low permittivity, the degradation constant is smaller than when muscle and skin conditions have high conductivity and high permittivity. The estimated values of E1 and E2 at the various sites indicated in hyperref[Fig.04]Figs. 4, 5, and 6 are displayed Table 4. E-field and E-field deterioration for various conductivity metrics differ in that, in Table 3, E_2 and E_1 are nearly identical to the $S_A/S_P + L_Z$ value under various conductivity situations.

Table 3. Assessment of signal attenuation due to human body absorption.

Part	**b**	**Z** (m)	e^{-2bZ}	**Lz** (dB)
Muscle	12.64	—	0.41	-3.87
Skin	12.31	0.035	0.42	-3.76
Fat	10.42	—	0.48	-3.19

According to Table 4 findings, electric field degradations are greater in higher conductivity and permittivity media, such as muscle and skin conditions, due to greater absorption loss. (Wang et al., 2022). The surface-area ratio S_A/S_P was computed geometrically using the antenna physical dimensions and phantom geometry, as defined in Eqs. 3, 4, 5, 6 and 7.

Table 4. Electric field spatial spread overview.

Parameter	**Muscle**		**Skin**		**Fat**	
σ (S/m)	00.00	00.79	00.00	00.69	00.00	00.119
E_1 (dB)	51.00	44.00	70.00	65.00	80.00	70.00
E_2 (dB)	24.00	12.00	42.00	35.00	60.00	46.00
$E_2 - E_1$ (dB)	-27.00	-32.00	-28.00	-30.00	-20.00	-24.00
S_A/S_P (dB)	-27.00	-27.00	-26.60	-26.60	-19.72	-19.72
L_Z (dB)	00.00	-03.87	00.00	-03.76	00.00	-03.19
$S_A/S_P + L_Z$ (dB)	-27.00	-31.00	-26.60	-30.00	-19.72	-23.00

The attenuation term $L_Z was$ derived from the exponential decay model of the electric field along the propagation distance Z, using the degradation constant obtained from the logarithmic difference between E_1 and E_2. Compared with earlier implantable antenna studies, this work provides explicit numerical values for electric-field degradation rather than only qualitative trends or SAR-based observations. In this study, the electric field is reduced by approximately -32 dB in muscle and -20 dB in fat over a propagation depth of 35 mm. These values are higher than the field reductions typically reported or implied in previous homogeneous-phantom studies at similar frequencies, where attenuation is often in the range of 15 $\rightarrow$ 25 dB and not directly quantified. The attenuation constants obtained in this work (about 10.4 $\rightarrow$ 12.6N_p/m) are consistent with high-loss biological tissues and clearly demonstrate the stronger absorption in muscle compared to fat. By directly reporting field degradation, propagation depth, and attenuation constants, this study offers a clearer and more quantitative basis for comparing implantable antenna performance across different tissue environments. To validate the proposed propagation loss formulation, the analytically estimated attenuation values ($S_A/S_P + L_Z$) were directly compared with the electric-field degradation obtained from full-wave FEKO simulations. As shown in Table 4, the analytically predicted losses closely match the simulated values of E_2 - E_1 across all tissue types, with discrepancies typically within $1dB$. This agreement confirms that the proposed formulation captures the dominant physical mechanisms governing near-field attenuation in lossy biological media and provides a reliable quantitative model for comparing implantable antenna performance. Optimizing implantable antenna systems for wireless body-area networks (WBANs) requires an understanding of the behaviour of the electric field (E-field) and how it degrades under different conductivity conditions. A direct correlation between E-field strength and energy dissipation in biological tissues is demonstrated by Table 3, which shows that the E-field magnitudes, E_1 (near-field E-field at the antenna-tissue interface) and E_2 (far-field E-field after propagation through tissue), are roughly equivalent to the ratio of electric field spread on the surface of a phantom across various conductivity values. Figure 7 confirms that absorption and dielectric losses dominate E-field attenuation. These findings highlight the challenge of signal integrity in high-permittivity media, necessitating advanced antenna designs to mitigate degradation and enhance WBAN performance for biomedical applications.

4.4 Electromagnetic mechanisms governing electric-field degradation

The observed electric-field degradation in biological tissues is fundamentally governed by the combined effects of ohmic (conductive) loss and reactive near-field energy storage, both of which depend strongly on tissue conductivity (σ) and relative permittivity (ε_r). The degradation constant b, as reported in Table 3, increases with tissue conductivity, indicating enhanced electromagnetic energy dissipation within the medium. This behavior can be explained by the power dissipation density, given by Eq. 10.

$$P_{loss} = 0.5\sigma|E|^2 \tag{10}$$

where $|E|$ is the local electric-field magnitude. Tissues with higher conductivity, such as muscle ($\sigma = 0.79(S/m)$), dissipate electromagnetic energy more efficiently into heat, resulting in stronger attenuation of the propagating near-field. This explains the larger degradation constant and the observed $-32dB$ field reduction in muscle tissue. In contrast, fat tissue exhibits significantly lower conductivity ($\sigma = 0.119(S/m)$), leading to reduced ohmic losses and correspondingly lower electric-field degradation ($\approx 20dB$). As a result, fat provides a comparatively favourable propagation environment for implanted antennas. Beyond conductive loss, tissue permittivity plays a critical role in reactive near-field energy storage. High-permittivity tissues, such as muscle and skin ($\varepsilon_r > 45$), store a larger fraction of electromagnetic energy in the form of electric polarization. This stored reactive energy does not contribute to radiation but instead increases local field confinement near the antenna, intensifying absorption and reducing the effective radiated field. The combined influence of conductivity and permittivity can be described through the dielectric loss tangent, defined as in Eq. 11.

$$\tan(\delta) = \sigma/(\omega\varepsilon) \tag{11}$$

where ω is the angular frequency and ε is the absolute permittivity. Higher values of $tan(\delta)$, as encountered in muscle tissue, indicate stronger loss behaviour, leading to increased power dissipation and field attenuation. Conversely, fat tissue exhibits a lower loss tangent, resulting in reduced energy dissipation and improved field penetration.

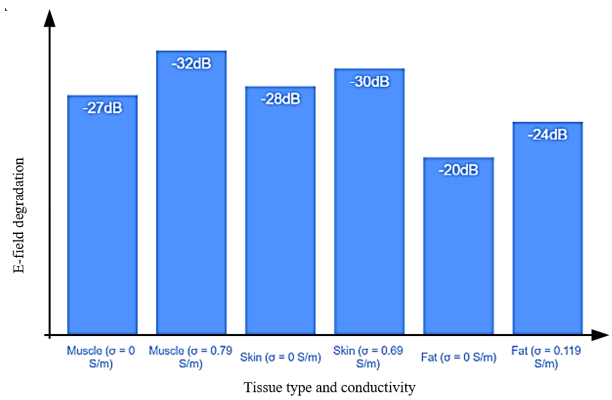

Figure 7. Assessment of Signal Attenuation Due to Human Body Absorption.

To elucidate the contributions of this study in calculating surface area and electric field spread for implantable antennas and elliptic cylindrical phantoms in wireless body-area networks (WBANs),Table 5 compares our work with three prior studies. The comparison focuses on methodology, antenna/phantom models, surface area calculations, E-field metrics, and key findings, highlighting how our approach using Eqs. 3, 4, 5, 6 and 7 to compute surface areas (S_A,S_P) and E-field spread ratios addresses limitations in earlier works, such as elliptic cylindrical phantom geometries and lack of detailed E-field spread analysis in biomedical contexts.

Table 5. Comparison of the current study with previous works.

Study	Antenna / Phantom	Surface Area Calculation	E-field Metrics	Key Findings
[18]	Cylindrical antenna, homogeneous phantom	$S_P = 2\pi rH$ (phantom only)	E-field magnitude, SAR	E-field decreases with distance, SAR higher in homogeneous tissue
Current Study	Patch antenna, elliptic cylindrical phantom	$S_A = L \times W$ $S_P = H \times D \times \pi$	E_1, E_2, S_A/S_P	E-field spread ratio ($SA/SP = -23dB$) correlates with tissue losses, detailed surface area analysis

5. Conclusion

The performance of a Meander Line Antenna (MLA) in body settings is greatly influenced by tissue characteristics, notably conductivity and permittivity, according to the findings of this study. The results show that because adipose tissue has a lower conductivity and permittivity than muscle and skin, it is a superior medium for implanted antennas because it deteriorates the electric field less. Higher conductivity tissues, including muscle, have higher propagation losses and signal attenuation, which may limit communication efficacy. The information suggests many doable strategies to improve antenna performance in biomedical applications, particularly in environments with high conductivity. These improvements can be achieved in a variety of ways. First, a structural alteration that improves antenna efficiency can lead to better performance in complex biological situations. Second, using state-of-the-art, biocompatible materials with improved electromagnetic characteristics may improve overall performance and reduce signal loss. Lastly, by carefully positioning the antenna in accordance with the composition of the surrounding tissues, signal degradation may be minimized. These results can be used to more effectively optimize future implanted antenna designs for wireless health monitoring tools and on-body communication systems, increasing the reliability and efficacy of biomedical communication systems. In order to reduce E-field degradation in different tissue types, we want to study multi-frequency antenna designs in the future using multi-layer phantoms.

Authors' contribution

All authors contributed equally to the preparation of this article.

Declaration of competing interest

The authors declare no conflicts of interest.

Funding source

This research is fully supported by Sunway University Early Career Research Grant, GRTIN-ECR (02)-DCIS-05-2024.

Data availability

The data that support the findings of this study are available from the corresponding author upon reasonable request.

Acknowledgements

The authors gratefully acknowledge the support and facilities provided by Universiti Teknologi Malaysia (UTM) during the course of this research.

REFERENCES

[1] A. Y. et al., "Implantable flexible sensors for health monitoring," *Advanced Healthcare Materials*, vol. 13, no. 2, p. 2302460, 2024. [Online]. Available: https://doi.org/10.1002/adhm.202302460

[2] B. Vandenberk and S. R. Raj, "Remote patient monitoring: what have we learned and where are we going?" *Current Cardiovascular Risk Reports*, vol. 17, no. 6, pp. 103–115, 2023. [Online]. Available: https://doi.org/10.1007/s12170-023-00720-7

[3] M. M. S. et al., "Review on medical implantable antenna technology and imminent research challenges," *Sensors*, vol. 21, no. 9, p. 3163, 2021. [Online]. Available: https://doi.org/10.3390/s21093163

[4] K. G. et al., "Evolution of wearable devices with real-time disease monitoring for personalized healthcare," *Nanomaterials*, vol. 9, no. 6, p. 813, 2019. [Online]. Available: https://doi.org/10.3390/nano9060813

[5] F. P. P. et al., "Antenna design and sar analysis on human head phantom simulation for future clinical applications," *Journal of Biomedical Science and Engineering*, vol. 10, no. 9, p. 421, 2017. [Online]. Available: https://doi.org/10.4236/jbise.2017.109032

[6] A. S. Poon, S. O'Driscoll, and T. H. Meng, "Optimal frequency for wireless power transmission into dispersive tissue," *IEEE Transactions on Antennas and Propagation*, vol. 58, no. 5, pp. 1739–1750, 2010. [Online]. Available: https://doi.org/10.1109/tap.2010.2044310

[7] E. A. Oshin, S. Guo, and C. Jiang, "Determining tissue conductivity in tissue ablation by nanosecond pulsed electric fields," *Bioelectrochemistry*, vol. 143, p. 107949, 2022. [Online]. Available: https://doi.org/10.1016/j.bioelechem.2021.107949

[8] I. S. M. et al., "Measurement of tissue optical properties in a wide spectral range: a review," *Biomedical Optics Express*, vol. 14, no. 1, pp. 249–298, 2022. [Online]. Available: https://doi.org/10.1364/boe.479320

[9] A. Gorst, K. Zavyalova, V. Yakubov, A. Mironchev, and A. Zapasnoy, "Theoretical simulation of the near-field probe for non-invasive measurements on planar layers with biological characteristics," *Bioengineering*, vol. 7, no. 4, p. 149, 2020. [Online]. Available: https://doi.org/10.3390/bioengineering7040149

[10] K. Aliqab, I. Nadeem, and S. R. Khan, "A comprehensive review of in-body biomedical antennas: Design, challenges and applications," *Micromachines*, vol. 14, no. 7, p. 1472, 2023. [Online]. Available: https://doi.org/10.3390/mi14071472

[11] S. Singh and D. Prasad, "Wireless body area network (wban): A review of schemes and protocols," *Materials Today: Proceedings*, vol. 49, pp. 3488–3496, 2022, national Conference on Functional Materials: Emerging Technologies and Applications in Materials Science. [Online]. Available: https://doi.org/10.1016/j.matpr.2021.05.564

[12] C. Origlia, D. O. Rodriguez-Duarte, J. A. T. Vasquez, J.-C. Bolomey, and F. Vipiana, "Review of microwave near-field sensing and imaging devices in medical applications," *Sensors*, vol. 24, no. 14, p. 4515, 2024. [Online]. Available: https://doi.org/10.3390/s24144515

[13] Y. Feng, Z. Li, L. Qi, W. Shen, and G. Li, "A compact and miniaturized implantable antenna for ism band in wireless cardiac pacemaker system," *Scientific Reports*, vol. 12, no. 1, p. 238, 2022. [Online]. Available: https://doi.org/10.1038/s41598-021-04404-3

[14] W. W. Tai, M. S. Zulkefli, and P. J. Soh, "A review of implantable and ingestible antenna for wireless capsule endoscopy system," in *AIP Conference Proceedings*, vol. 2579, no. 1, 2023. [Online]. Available: https://doi.org/10.1063/5.0115803

[15] S. Gabriel, R. Lau, and C. Gabriel, "The dielectric properties of biological tissues: Ii. measurements in the frequency range 10 Hz to 20 GHz," *Physics in Medicine and Biology*, vol. 41, no. 11, p. 2251, 1996.

[16] C. A. Balanis, *Antenna Theory: Analysis and Design*. John Wiley and Sons, 2016.

[17] J. E. S. et al., "A dataset of 3d structural and simulated transport properties of complex porous media," *Scientific Data*, vol. 9, no. 1, p. 579, 2022. [Online]. Available: https://doi.org/10.1038/s41597-022-01664-0

[18] A. Kiourti and K. S. Nikita, "A review of implantable patch antennas for biomedical telemetry: Challenges and solutions [wireless corner]," *IEEE Antennas and Propagation Magazine*, vol. 54, no. 3, pp. 210–228, 2012.

How to cite this article:
Ngu War Hlaing, Kamilia Kamardin, Yoshihide Yamada, and Angela Amphawan, (2026). 'Investigation of near field distributions of meander line antenna in human body conditions', Al-Qadisiyah Journal for Engineering Sciences, 19 (2), pp. 225- 230. `https://doi.org/10.30772/qjes.2026.165671.1756`